Accurate double many-body expansion potential energy surface by extrapolation to the complete basis set limit and dynamics calculations for ground state of NH 2

ARTICLE *in* JOURNAL OF COMPUTATIONAL CHEMISTRY · JULY 2013

Impact Factor: 3.59 · DOI: 10.1002/jcc.23310 · Source: PubMed

5 AUTHORS, INCLUDING:

Jiuchuang Yuan
Dalian University of Technology
10 PUBLICATIONS **25** CITATIONS
SEE PROFILE

Mengtao Sun
Chinese Academy of Sciences
130 PUBLICATIONS **2,777** CITATIONS
SEE PROFILE

Accurate Double Many-Body Expansion Potential Energy Surface by Extrapolation to the Complete Basis Set Limit and Dynamics Calculations for Ground State of NH_2

Yongqing Li,*[a] Jiuchuang Yuan,[b] Maodu Chen,*[b] Fengcai Ma,[a] and Mengtao Sun[c]

An accurate single-sheeted double many-body expansion potential energy surface is reported for the title system. A switching function formalism has been used to warrant the correct behavior at the $H_2(X^1\Sigma_g^+)+N(^2D)$ and $NH(X^3\Sigma^-)+H(^2S)$ dissociation channels involving nitrogen in the ground $N(^4S)$ and first excited $N(^2D)$ states. The topographical features of the novel global potential energy surface are examined in detail, and found to be in good agreement with those calculated directly from the raw *ab initio* energies, as well as previous calculations available in the literature. The novel surface can be using to treat well the Renner–Teller degeneracy of the $1^2A''$ and $1^2A'$ states of NH_2. Such a work can both be recommended for dynamics studies of the $N(^2D)+H_2$ reaction and as building blocks for constructing the double many-body expansion potential energy surface of larger nitrogen/hydrogen-containing systems. In turn, a test theoretical study of the reaction $N(^2D)+H_2(X^1\Sigma_g^+)(v=0,j=0) \rightarrow NH(X^3\Sigma^-)+H(^2S)$ has been carried out with the method of quantum wave packet on the new potential energy surface. Reaction probabilities, integral cross sections, and differential cross sections have been calculated. Threshold exists because of the energy barrier (68.5 meV) along the minimum energy path. On the curve of reaction probability for total angular momentum $J = 0$, there are two sharp peaks just above threshold. The value of integral cross section increases quickly from zero to maximum with the increase of collision energy, and then stays stable with small oscillations. The differential cross section result shows that the reaction is a typical forward and backward scatter in agreement with experimental measurement result. © 2013 Wiley Periodicals, Inc.

DOI: 10.1002/jcc.23310

Introduction

The amidogen (NH_2) radical plays a crucial role in atmospheric chemistry and combustion processes, being also a prototype in spectroscopic and reaction dynamics studies. NH_2 is a well-established prototype for the study of insertion reactions, with the reaction $N(^2D)+H_2(X^1\Sigma_g^+)$ also playing a key role in the combustion of nitrogen-containing materials. During the past decade, the reaction $N(^2D)+H_2(X1\Sigma_g^+) \rightarrow NH(X^3\Sigma^-)+H(^2S)$ has been much studied both experimentally[1–5] and theoretically.[6–20] There are five electronic doublet states correlating with the title reaction, and this reaction is a prototype for studying nonadiabatic effect. The Coriolis coupling effect in nonadiabatic dynamics is important in some molecular reaction dynamics[21–24], and Chu et al.[17] found this effect plays a small role in the reaction of $N(^2D)+H_2(X1\Sigma_g^+) \rightarrow NH(X^3\Sigma^-)+H(^2S)$. Most studies of the title system have been carried out on its ground electronic adiabatic state potential energy surface (PES) and first excited state (labeled $1^2A''$ and $1^2A'$ in C_s symmetry, respectively). These PESs form a Renner–Teller (RT) pair of $^2\Pi_u$ character at linear geometries, with both PESs becoming degenerate at some linear $D_{\infty h}$ and $C_{\infty v}$ geometries and at the asymptote, $N(^2D)+H_2(X^1\Sigma_g^+)$. Amongst the theoretical studies, the $N(^2D)+H_2(X1\Sigma_g^+) \rightarrow NH(X^3\Sigma^-)+H(^2S)$ reaction has been studied using a LEPS (London–Eyring–Polanyi–Sato) PES proposed by Suzuki et al.,[11] and a more realistic form obtained by fitting *ab initio* data to a Sorbie–Murrell type function.[25] Ho et al.[26] reported the PES for the ground state of NH_2 by using the reproducing kernel Hilbert space (RKHS) interpolation method. Pederson et al.[27,28] reported accurate *ab initio* calculations and global PESs for the ground ($12A''$) and first excited ($12A'$) electronic states using an interpolation technique known as RKHS. They reveal the degeneracy at linear HNH geometries forming a RT coupled pair of $^2\Pi$ symmetry. In turn, calculations of PESs for the above two electronic states of NH_2 have also been performed by Qu et al.[14] using the multireference configuration interaction (MRCI) approach, mostly with the aug-cc-pV *QZ*

[a] *Y. Li, F. Ma*
Department of Physics, Liaoning University, Shenyang, 110036, China
E-mail: yqli@lnu.edu.cn
[b] *J. Yuan, M. Chen*
School of Physics and Optoelectronic Technology, Dalian University of Technology, Dalian, 116024, China
E-mail: mdchen@dlut.edu.cn
[c] *M. Sun*
Beijing National Laboratory for Condensed Matter Physics, Institute of Physics, Chinese Academy of Sciences, Beijing, 100190, China

Contract/grant sponsor: National Natural Science Foundation of China; Contract/grant number: 11274149, 10974023; Contract/grant sponsor: National Science Foundation of Liaoning Province; Contract/grant number: 20121032; Contract/grant sponsor: Program of Shenyang Key Laboratory of Optoelectronic materials and technology; Contract/grant number: F12-254-1-00

(such basis are generally denoted as AV *XZ*, with *X* being usually referred to as the basis set cardinal number) and cubic-spline fits for the representation. Moreover, Zhou et al.[29] reported a global PES for $NH_2(12A'')$ based on high-level *ab initio* points, which were performed at the MRCI(Q) level (MRCI with the Davidson correction) using an AV *QZ* basis set.

Varandas and Poveda[16] reported a single-sheeted double many-body expansion (DMBE) PES for the ground state $1^2A''$ state of NH_2 from MRCI *ab initio* energies, using the double many-body expansion-scaled external correlation (DMBE/SEC)[30] to slightly correct the semiempirically calculated raw energies. To take care of the dissociation channels involving nitrogen in the ground $N(^4S)$ and first $N(^2D)$ excited states, a switching-function formalism has been utilized. Chu et al.[17] reported a dynamics study of the reaction $N(^2D)+H_2(v=0,j=1-5) \rightarrow NH(X^3\Sigma^-)+H(^2S)$ using the time-dependent quantum wave packet method and the DMBE/SEC PES for $NH_2(1^2A'')$. Moreover, Li and Varandas[31] reported two single-sheeted DMBE PESs for the $1^2A'$ state based on the DMBE/SEC method and complete basis set (CBS) extrapolation[32], respectively. To treat the RT degeneracy, a three-dimensional switching function has been utilized to ensure an accurate match of both 12A″ and 12A′ DMBE/SEC PESs at linear $D_{\infty h}$ geometries. However, as noted in Ref. [31], due to the small difference between the $NH_2(1^2A'')$ DMBE/SEC and 12A′ DMBE/CBS values of the $N(^2D)$ energy, they suggested first by applying the above procedure to warrant the RT degeneracy of the 12A″ DMBE/SEC PES and the 12A′ DMBE/CBS PESs, and then using a procedure similar to this to impose degeneracy at the $N(^2D)+H_2(X^1\Sigma_g^+)$ asymptote. But this second step should lead to an extra error of the 12A′ DMBE/CBS barrier relative to the $N(^2D)+H_2(X^1\Sigma_g^+)$ asymptote. This situation promoted us to fitting a 12A″ DMBE/CBS PES to ensure an accurate match of both DMBE/CBS PESs at linear $D_{\infty h}$ geometries and at $N(^2D)+H_2(X^1\Sigma_g^+)$ asymptotic regions, and do not lead to an extra error of the 12A′ DMBE/CBS barrier relative to the $N(^2D)+H_2(X^1\Sigma_g^+)$ asymptote.

The major goal of the present work is, therefore, to report an accurate global PES for $NH_2(12A'')$ based on DMBE/CBS method [31,33,34]. The popular Davidson correction has also been employed to account for quadruple excitations, MRCI(Q). Both AV *TZ* and AV *QZ* atomic basis sets of Dunning [35] have been employed. As it is well known, to obtain a chemically accurate PES, very large basis sets are usually required. In this work, rather than utilizing such huge basis sets, we have extrapolated the total energy to the CBS limit by employing the uniform singlet-pair and triplet-pair (USTE[32,36]) scheme. The novel PES can be used to treat well the RT degeneracy of the 12A′ and 12A″ DMBE/CBS PESs. In turn, this work can both be recommended for dynamics studies of the $N(^2D)+H_2$ reaction and as building blocks for constructing the DMBE/CBS PESs of larger nitrogen/hydrogen-containing systems.

The article is organized as follows. The section entitled Ab initio Calculations and Extrapolation Scheme describes the *ab initio* calculations, while the analytical representation of the PES is reported in the section Single-Sheeted DMBE Potential Energy Surface. The main topographical features of the $NH_2(12A'')$ adiabatic PES will be examined in the section Features of $NH_2(12A'')$ Potential Energy Surface. In section entitled Quantum Wave Packet Dynamics Study Performed for the $N(^2D)+H_2(X^1\Sigma_g^+)$ Reaction, an accurate quantum mechanical method using time-dependent wave packet (TDWP) is carried out on the reaction of $N(^2D)+H_2(X^1\Sigma_g^+)(v=0,j=0) \rightarrow NH(X^3\Sigma^-)+H(^2S)$. Some conclusions are gathered under section Concluding Remarks.

Ab initio Calculations and Extrapolation Scheme

To map the PES, a total of 2102 points have been calculated for $N-H_2$ regions defined by $1.2 \le R_{H_2}/a_0 \le 3.6$, $1.4 \le r_{N-H_2}/a_0 \le 10$, and $0 \le \gamma/\text{deg} \le 90$ while, for H−NH, they cover geometries defined by $1.8 \le R_{NH}/a_0 \le 3.6$, $1.4 \le r_{H-NH}/a_0 \le 10$, and $0 \le \gamma/\text{deg} \le 180$; *R*, *r*, and γ are atom–diatom Jacobi coordinates. All *ab initio* calculations have been carried out at the MRCI(Q)[37,38] level with the MOLPRO[39] package, using the full valence complete active space (FVCAS)[37] wave function as reference. The state averaging of the two lowest states of the same $^2A''$ symmetry have been used, since there not the RT-pairing if only doing a single-state calculation. The AV *TZ* and AV *QZ* atomic basis sets of Dunning[35] have been employed. This involves seven correlated electrons in six active orbitals (5A′+1A″), amounting to a total of 92 (62A′+30A″) and 172 (110A′+62A″) configuration state functions at AV *TZ* and AV *QZ* atomic basis sets, respectively. To accelerate convergence of the correlation energy to the one-electron CBS limit, the USTE[32] scheme is employed. In all calculations, the core is kept frozen and relativistic effects are ignored.

Built in a systematic manner that is intended to relate the correlation energy to the cardinal number *X*, Dunning's correlation consistent basis sets allow the extrapolation of the raw energies to the one-electron CBS limit. To perform the extrapolation, the MRCI(Q) energy is treated as usual in split form by writing[32]

$$E_X(\mathbf{R}) = E_X^{\text{CAS}}(\mathbf{R}) + E_X^{\text{dc}}(\mathbf{R}) \quad (1)$$

where the subscript *X* indicates that the energy has been calculated in the AV *XZ* basis, and the superscript dc stands for the dynamical correlation energy. Note that all extrapolations are carried pointwise, and hence the vector **R** of the nuclear geometrical coordinates will be omitted for simplicity.

To extrapolate the complete active space (CAS) energy (uncorrelated in the sense of lacking dynamical correlation), a proposed[32] generalization of the protocol adopted by Karton and Martin[40] (KM) to extrapolate single-reference self-consistent-field energies is utilized,

$$E_X^{\text{CAS}} = E_\infty^{\text{CAS}} + B/X^\alpha \quad (2)$$

where α is a predefined constant. Being a two-parameter protocol (E_∞^{CAS}, B), a minimum of two raw energies will be required for the extrapolation. Specifically, eq. (2) will be calibrated from the CAS/AV(*T*, *Q*)Z energy pairs, using a value of $\alpha=5.34$ which has been found optimal when extrapolating extended-hartree-Fock (EHF) energies to the CBS limit.

Table 1. Parameters for two-body potential energy curves of NH ($X^3\Sigma^-$).

Parameter	NH ($X^3\Sigma^-$)
R_e/a_0	1.960
D/E_h	0.231295
α_1/a_0^{-1}	3.6075
α_2/a_0^{-2}	4.22711
α_3/a_0^{-3}	1.7834
γ_0/a_0^{-1}	3.02313
γ_1/a_0^{-1}	−0.126214
γ_2/a_0^{-1}	1.31923
R_0/a_0	6.9282032
$C_6/E_h a_0^{-6}$	12.27
$C_8/E_h a_0^{-8}$	232.6
$C_{10}/E_h a_0^{-10}$	5775.0

In the present work, we will then utilize the USTE/(T,Q) scheme to extrapolate the dynamical correlation energy. For the dynamical correlation, a popular protocol is[41]

$$E_X^{dc} = E_\infty^{dc} + \frac{A_3}{(X+\alpha)^3} + \frac{A_5}{(X+\alpha)^5} \quad (3)$$

with the auxiliary relation

$$A_5 = A_5(0) + cA_3^m \quad (4)$$

where E_∞, $A_5(0)$, A_3, c, m, and α are parameters. The numerical values of the parameters in eq. (3) are dependent on the *ab initio* method and can be obtained by consulting Table 1 of Ref. [32]. In fact, the method has since been successfully utilized for a variety of other systems,[31–34,42–47] with the reader being addressed to such papers for further details.

Single-Sheeted DMBE Potential Energy Surface

Within the framework of DMBE theory[16,48], the single-sheeted PES is written as

$$V(\mathbf{R}) = \sum_{i=1}^{3} V^{(i)}(\mathbf{R}) \quad (5)$$

where **R** is the vector of the three internuclear coordinates $[R_j(j=1,\ldots,3)]$, $V^{(1)} = V_{N(^2D)} f(\mathbf{R})$ is a one-body term, $V_{N(^2D)}$ represents the energy difference between the ^{2}D and ^{4}S states of atomic nitrogen once extrapolated to the CBS limit: $V_{N(^2D)} = 0.0868702 E_h$. This should be compared with the result obtained by Varandas et al.[16] from MRCI/AV *QZ* energies at the cheaper single-state level, $V_{N(^2D)} = 0.09014 E_h$, which is ~2kcal mol^{-1} larger than our result. In turn, $f(\mathbf{R})$ is the switching function used to warrant the correct behavior of the $H_2(X^1\Sigma_g^+) + N(^2D)$ and $NH(X^3\Sigma^-) + H(^2S)$ dissociation limits. In this work, the one-body switching function assumes the form[16]

$$f(\mathbf{R}) = h(R_1) g(r_1) \quad (6)$$

where

$$h(R_1) = \frac{1}{4} \sum_{i=1}^{2} \left\{ 1 - \tanh\left[\alpha_i \left(R_1 - R_1^{i0} \right) + \beta_i \left(R_1 - R_1^{i1} \right)^3 \right] \right\} \quad (7)$$

$$g(r_1) = \frac{1}{2} \left\{ 1 + \tanh\left[\alpha_0 \left(r_1 - r_1^0 \right) \right] \right\} \quad (8)$$

where R_1 represents the H−H distance, r_1 is the distance of the N atom to the center of mass of H_2. All numerical values of the parameters in eq. (6) have been taken from Ref. [16] for the DMBE/SEC PES of ground state NH_2, with the notation and numerical values kept unchanged to prevent any confusion. As we can see from Figure 1, we use the one-body switching function to control the $N(^2D) - N(^4S)$ decay as the H−H distance increases for $N + H_2$ isosceles configurations.

$V^{(2)}$ and $V^{(3)}$ represent the two-body and three-body energy terms, respectively. The following sections give the details of analytical forms employed to represent the switching function, and two-body and three-body energy terms used in the present work. As usual in the DMBE formalism, the EHF contributions are calibrated by fitting *ab initio* data to a suitable, physically motivated, functional form. In turn, the dc energies are modeled to a function that uses *ab initio* long-range dispersion energy (as well as electrostatic and induction when judged relevant) coefficients, eventually estimated at the same level of *ab initio* theory. Thus, no empirical information is required for the construction of the final PES using DMBE theory.

The potential energy curves for the two-body fragments are based on the extended Hartree–Fock approximate correlation energy method for diatomic molecules including the united atom limit[49] (EHFACE2U)which show the correct behavior at both asymptotic limits $R \to 0$ and $R \to \infty$.

For a slightly improved accuracy, the EHFACE2U potential energy curve for the ground state $H_2(X^1\Sigma_g^+)$ reported in Ref. [50] has been adopted in the present work. For imidogen, $NH(X^3\Sigma^-)$, the potential curve has been chosen to mimic the MRCI/CBS *ab initio* energies here reported. All parameters are gathered in Table 1. As shown in Figure 2, both potential curves mimic accurately the MRCI/CBS *ab initio* calculated in the present work.

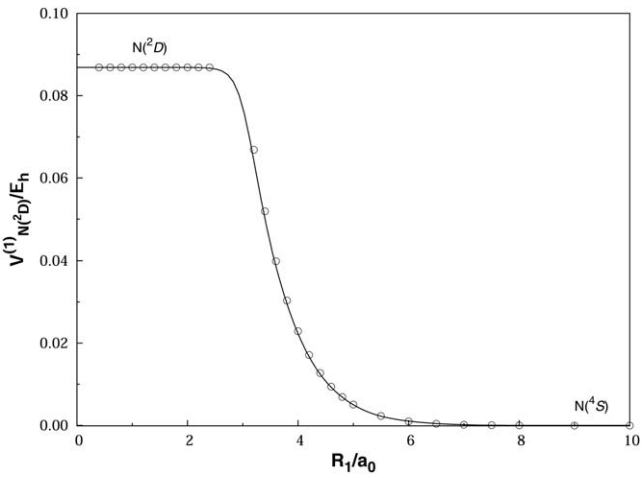

Figure 1. Shown the CBS/MRCI(Q) *ab initio* energies and the switching function used to model the single-sheeted NH_2 DMBE/CBS PES for $N + H_2$ configuration as a function of H−H distance R_1.

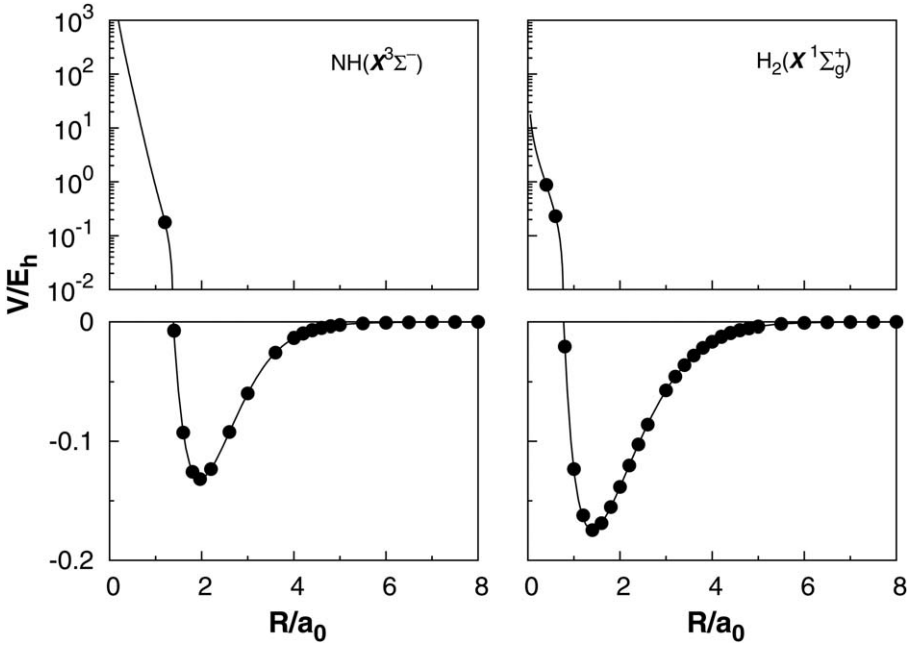

Figure 2. EHFACE2U potential energy curves for NH $(X^3\Sigma^-)$ and $H_2\left(X^1\Sigma_g^+\right)$. The solid dots indicate the CBS/MRCI(Q) *ab initio* points calculated in the present work.

The three-body energy is written as

$$V^{(3)}(\mathbf{R}) = V^{(3)}_{\mathrm{EHF}}(\mathbf{R}) + V^{(3)}_{\mathrm{dc}}(\mathbf{R}) \tag{9}$$

where $V^{(3)}_{\mathrm{EHF}}$ and $V^{(3)}_{\mathrm{dc}}$ are the three-body terms of extended Hartree–Fock and dynamical correlation energy, respectively.

The three-body dynamical correlation is written as[50]

$$V^{(3)}_{\mathrm{dc}} = -\sum_i \sum_n f_i(\mathrm{R}) C^{(i)}_n(R_i, \theta_i) \chi_n(r_i) r_i^{-n} \tag{10}$$

where r_i, θ_i and R_i are the Jacobi coordinates corresponding to a specific atom–diatom arrangement of the triatomic and $f_i = \frac{1}{2}\{1 - \tanh[\xi(\eta R_i - R_j - R_k)]\}$ is a switching function. Following our recent work on $NH_2(1^2A'')$[16] and $NH_2(1^2A')$[31], the parameters have been fixed at $\eta = 6$, $\xi = 1.0 a_0^{-1}$, and $\rho = 16.125 a_0$. In turn, the atom–diatom dispersion coefficients in eq. (10) assume their typical form

$$C^{(i)}_n(R_i) = \sum_L C^L_n(R) P_L(\cos\theta_i) \tag{11}$$

where $P_L(\cos\theta_i)$ denotes the Lth Legendre polynomial. The expansion in eq. (11) has been truncated by considering only the coefficients C^0_6, C^2_6, C^0_8, C^2_8, C^4_8, and C^0_{10}; all other coefficients are assumed to make a negligible contribution, and hence neglected. As usual, the atom–diatom dispersion coefficients assume the form

$$C^{L,\mathrm{A-BC}}_n(R) = C^{L,\mathrm{AB}}_n + C^{L,\mathrm{AC}}_n + D_M \left(1 + \sum_{l=1}^{3} a_i r^i\right) \exp\left(\sum_{l=1}^{3} b_i r^i\right) \tag{12}$$

As eq. (11) is known to cause an overestimation of the dynamical correlation energy at the atom–diatom dissociation channels.[50] The two-body dynamical correlation energy for the ith pair has been multiplied by $\Pi_{j\neq i}(1-f_j)$. This ensures[50,51] that the only two-body contribution at the ith channel will be by the jk one. The parameters in eqs. (10–12) have been taken from Ref. [16] for ground state NH_2, with the notation and numerical values kept unchanged to prevent any confusion.

By removing, for a given triatomic geometry, the sum of the one- and two-body energy terms from the corresponding interaction energies, one obtains the total three-body energy. By then, subtracting the three-body dynamical correlation contribution in eq. (10) from the total three-body energy, the three-body EHF energy contribution is obtained. This has been modeled via the three-body distributed-polynomial[16,52] form

$$V^{(3)}_{\mathrm{EHF}} = \sum_{j=1}^{3} \left\{ P^{(j)}(Q_1, Q_2, Q_3) \prod_{i=1}^{3} \left\{ 1 - \tanh\left[\gamma^{(j)}_i \left(R_i - R^{(j)}_{i,\mathrm{ref}}\right)\right]\right\}\right\} \tag{13}$$

where the polynomial $P^{(j)}(Q_1, Q_2, Q_3)$ is the jth polynomial, with $Q_i (i = 1-3)$, being the symmetry coordinates, defined as[52–55]

$$\begin{bmatrix} Q_1 \\ Q_2 \\ Q_3 \end{bmatrix} = \begin{bmatrix} \sqrt{1/3} & \sqrt{1/3} & \sqrt{1/3} \\ \sqrt{1/2} & -\sqrt{1/2} & 0 \\ -\sqrt{1/6} & -\sqrt{1/6} & \sqrt{2/3} \end{bmatrix} \begin{bmatrix} R_1 - R^{(j)}_{1,\mathrm{ref}} \\ R_2 - R^{(j)}_{2,\mathrm{ref}} \\ R_3 - R^{(j)}_{3,\mathrm{ref}} \end{bmatrix} \tag{14}$$

In turn, $R^{(j)}_{i,\mathrm{ref}}$ is a reference geometry and $\gamma^{(j)}_i$ the nonlinear range-determining parameters that have been optimized via a trial-and-error procedure that minimizes the root-mean-squared deviation (RMSD) error while warranting the proper

Table 2. Parameters and reference geometries of DMBE PES in the extended Hartree–Fock energy of eq. (17).

Coefficients	<aip-mml>$P^{(1)}$	$P^{(2)}$	$P^{(3)}$
$\gamma_1^{(j)}/a_0^{-1}$	1.5	2.5	3.5
$\gamma_2^{(j)}/a_0^{-1}$	4.0	3.0	3.5
$\gamma_3^{(j)}/a_0^{-1}$	4.0	3.0	3.5
$R_1^{(j),\mathrm{ref}}/a_0$	0.8	1.1	1.0
$R_2^{(j),\mathrm{ref}}/a_0$	0.9	0.6	1.0
$R_3^{(j),\mathrm{ref}}/a_0$	0.9	0.6	1.0

Table 3. Numerical values of DMBE/CBS PES, which used in the extended Hartree–Fock energy in eq. (17).

Coefficients	$P^{(1)}$	$P^{(2)}$	$P^{(3)}$
C_1/a_0^0	−1.5809222552	3.8205409058	−1.1162398248
C_2/a_0^{-1}	−1.7297792423	0.0233578114	−0.0132125249
C_3/a_0^{-1}	0.8765463020	−0.5994963337	0.0321696124
C_4/a_0^{-2}	−0.3255169992	0.8830575945	−0.4824779926
C_5/a_0^{-2}	0.0421378365	1.3701734919	−0.4793246898
C_6/a_0^{-2}	1.6134271596	1.0632284500	0.2328557585
C_7/a_0^{-2}	−0.7744794351	−0.5789068003	−0.1028274211
C_8/a_0^{-3}	−0.3729177393	0.0357336771	−0.0258371789
C_9/a_0^{-3}	−0.6113508845	0.0520945789	0.0337264911
C_{10}/a_0^{-3}	−0.1511343470	0.0131941233	−0.0024269514
C_{11}/a_0^{-3}	0.6808533196	0.2173328153	0.1537390742
C_{12}/a_0^{-3}	0.1614269693	−0.1314866041	−0.0955324260
C_{13}/a_0^{-3}	−0.1211894557	0.1459518208	−0.0609409360
C_{14}/a_0^{-4}	0.0232674006	0.0503108880	−0.0766361025
C_{15}/a_0^{-4}	0.0799150085	0.0011279133	0.0381423103
C_{16}/a_0^{-4}	0.1131646991	0.1044931307	−0.0584822261
C_{17}/a_0^{-4}	−0.0527893396	−0.1545474364	0.0706134609
C_{18}/a_0^{-4}	0.3910057333	−0.0822490249	0.0718846349
C_{19}/a_0^{-4}	−0.0917034944	0.1801709939	−0.0455490296
C_{20}/a_0^{-4}	0.3419424886	−0.0742238026	−0.0414537007
C_{21}/a_0^{-4}	−0.0483999774	−0.0490824810	−0.0005093202
C_{22}/a_0^{-4}	−0.2581678243	−0.0556267653	0.0164127273
C_{23}/a_0^{-5}	−0.0197347467	0.0075198631	−0.0042041548
C_{24}/a_0^{-5}	−0.0707368093	0.0402735040	0.0252303237
C_{25}/a_0^{-5}	−0.1152914540	0.1271960667	0.0033194559
C_{26}/a_0^{-5}	−0.0152988582	0.0679298868	0.0058973034
C_{27}/a_0^{-5}	−0.0271410173	0.0396936340	0.0055574210
C_{28}/a_0^{-5}	0.0249910597	0.0360537017	0.0259301181
C_{29}/a_0^{-5}	0.1492601309	−0.0701997238	−0.0236910225
C_{30}/a_0^{-5}	−0.1352245312	0.2350464125	−0.0065666633
C_{31}/a_0^{-5}	−0.0672666345	0.0580154199	0.0183475655
C_{32}/a_0^{-5}	0.0264633265	−0.1188177099	0.0027405358
C_{33}/a_0^{-5}	−0.0688044342	0.1056976701	−0.0030041155
C_{34}/a_0^{-5}	−0.0056786670	−0.0115439286	−0.0007888098
C_{35}/a_0^{-6}	−0.0002239298	0.0067913466	−0.0039453382
C_{36}/a_0^{-6}	−0.0114475849	0.0049882455	0.0146400415
C_{37}/a_0^{-6}	0.0098955818	−0.0052794447	0.0010368802
C_{38}/a_0^{-6}	0.0242596042	0.0093474982	−0.0014363359
C_{39}/a_0^{-6}	0.0013153743	−0.0136621284	0.0106037485
C_{40}/a_0^{-6}	0.0042060488	−0.0040940195	0.0016192679
C_{41}/a_0^{-6}	−0.0002910064	0.0006484082	−0.0006020809
C_{42}/a_0^{-6}	0.0027145775	0.0050410560	0.0055907119
C_{43}/a_0^{-6}	−0.0026102898	−0.0034395695	−0.0056686084
C_{44}/a_0^{-6}	0.0157324066	0.0164825174	0.0035189003
C_{45}/a_0^{-6}	0.0147596846	0.0017609802	0.0069232298
C_{46}/a_0^{-6}	0.0012487139	−0.0008692250	−0.0039631300
C_{47}/a_0^{-6}	0.0138686024	−0.0212789750	0.0048618628
C_{48}/a_0^{-6}	0.0053795114	0.0030910903	−0.0008031266
C_{49}/a_0^{-6}	0.0045228023	−0.0100768855	0.0021026032
C_{50}/a_0^{-6}	−0.0042303305	0.0004612180	−0.0012211655

asymptotic behavior on dissociation. The complete set of parameters totals 150 linear coefficients, 9 nonlinear ones, and 9 reference bond distances. Table 2 gathers the reference geometries and nonlinear range-determining parameters, while Table 3 collects the linear ones. Table 4 shows the partial and accumulated stratified RMSD of the final DMBE/CBS PES with respect to all the fitted CBS/MRCI(Q) *ab initio* energies. As shown, a total of 2102 points covering an energy range of over 320kcal mol^{-1} above the $NH_2(12A'')$ global minimum has been utilized in the least-squares fit with special weights, which is a usual calibration procedure during fitting PES, having been attributed to the points close to stationary points. The fit shows that the total RMSD is 0.695mol^{-1}.

Features of $NH_2(12A'')$ Potential Energy Surface

The optimized C_{2v} bending curve of the $NH_2(12A'')$ DMBE/CBS PES is displayed in panel (a) of Figure 3 as a function of the bending angle, with the bond distance of NH optimized at each angle. Also shown for comparison in this figure is the bending curve of the accurate DMBE/SEC PES. Note that the barrier to linearity calculated from the DMBE/CBS PES is $11,630\mathrm{cm}^{-1}$, thus, $144\mathrm{cm}^{-1}$ smaller than the empirical result obtained from the effective one-dimensional bending potential model of Duxbury et al.[56]. It may also be compared well with that of $11,802\mathrm{cm}^{-1}$ obtained from the DMBE/SEC PES by Varandas et al.,[16] which is predicted to be only $172\mathrm{cm}^{-1}$ smaller. The near parallel behavior of the DMBE/CBS and DMBE/SEC PESs is highlighted in the bottom panel of Figure 3a, with DMBE/CBS predicting a slightly deeper well depth. This may largely be due to the fact that the DMBE-SEC method employs a single constant scaling factor for all points calculated with the AV *QZ* basis set at the cheaper single-state level. It may

Table 4. Accumulated (acc.) and stratum (strat.) root-mean-square deviations in kcal mol^{-1} of DMBE PES.

Energy		N[a]		Max. dev.[b]		RMSD		$N_{>\mathrm{rmsd}}$[c]	
Acc.	Strat.	Acc.	Strat.	Acc.	Strat.	Acc.	Strat.	Acc.	Strat.
10	0–10	129	129	0.149	0.149	0.022	0.022	9	9
20	10–20	138	9	0.633	0.633	0.088	0.333	11	4
30	20–30	152	14	1.122	1.122	0.205	0.615	18	6
40	30–40	176	24	1.178	1.178	0.282	0.564	30	8
50	40–50	201	25	1.472	1.472	0.392	0.823	41	11
60	50–60	222	21	1.894	1.894	0.445	0.786	49	6
70	60–70	258	36	1.894	1.639	0.525	0.868	65	15
80	70–80	286	28	2.393	2.393	0.562	0.830	72	9
90	80–90	338	52	2.393	2.205	0.604	0.795	92	13
100	90–100	417	79	2.393	2.110	0.618	0.676	113	21
150	100–150	1679	1262	4.798	4.798	0.619	0.619	315	202
200	150–200	2078	399	4.798	3.575	0.678	0.887	434	92
250	200–250	2091	13	4.798	2.378	0.685	1.360	437	5
300	250–300	2099	8	4.798	2.032	0.686	0.979	438	2
320	300–320	2102	3	4.798	3.589	0.695	2.980	430	2

[a] Number of calculated MRCI(Q)/CBS points up to the indicated energy range.
[b] Maximum deviation up to the indicated energy range. [c] Number of calculated MRCI(Q)/CBS points with an energy deviation larger than the root-mean-square deviation.

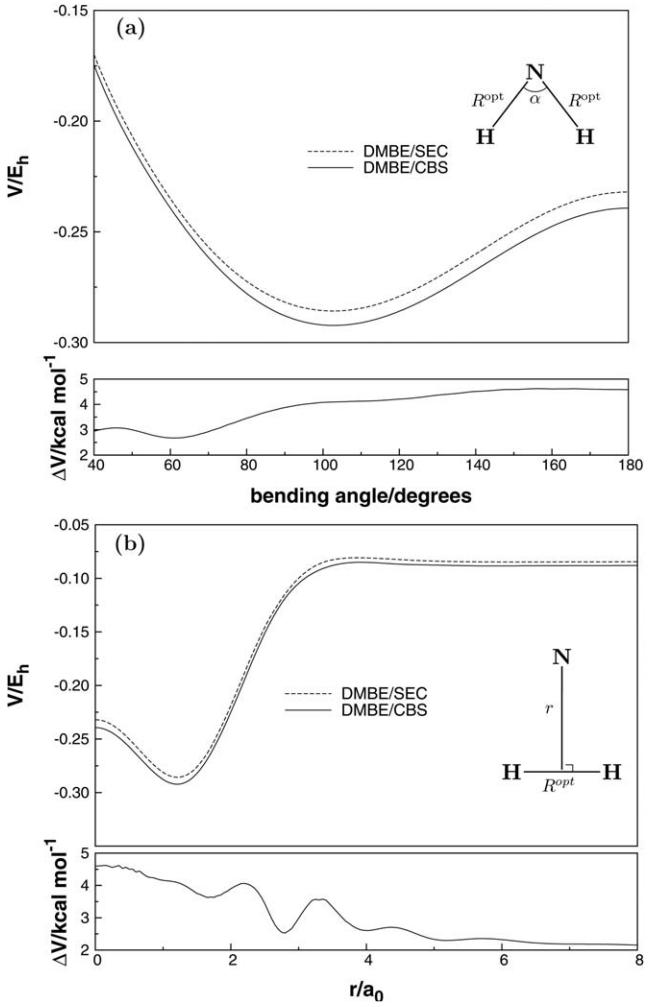

Figure 3. (a) Optimized C_{2v} bending curve of $NH_2(12A'')$ as a function of the bending angle, with the bond distance of NH optimized at each bending angle. (b) Approximate minimum energy path as a function of *r* (distance between the N atom and the center of the H—H diatom), with the H—H bond length optimized at each value of *r*.

also be due to the fact that the MRCI energies utilized to calibrate the DMBE/CBS form include the Davidson correction using state averaging of the two lowest states of the same $^2A''$ symmetry. This suggests that the DMBE-SEC scheme slightly underestimates such a popular correction, a finding also supported from our recent work on the ground state NH_2[16] and SH_2[33] systems. Quantitatively, the energy difference at the global minimum in Figure 3 amounts to $\sim$2kcal mol^{-1}, with the well depths calculated relative to the three-atom dissociation limit being $-0.2923E_h$ and $-0.2858E_h$ for the DMBE/CBS and DMBE/SEC PESs, respectively. Not surprisingly, as seen from panel (b) of Figure 3, the parallelism noted above largely disappears when one considers the optimized path for insertion of $N(^2D)$ into H_2. This is likely attributable to the very nature of the least-squares fit as the deviations fall on average close to the values given above. It may also be due to the fact that the special weights having been attributed to the points close to stationary points in the least-squares fitting procedure. The above results then corroborate the high reliability and consistency of the CBS and DMBE-SEC methods. Needless to say, it cannot be discarded that the above differences may also partly be attributable to the fact that core correlation effects are absent in the CBS energies while they are effectively taken into account in the empirical SEC correction. As pointed elsewhere,[31] one should further recall that other effects, often of competitive magnitude, are altogether also neglected, namely, relativistic and nonadiabatic ones. A final pragmatic reason for improving cost-effectiveness of the calculations stems from the observation that the data are going to be modeled with an accuracy that probably falls close to or even exceeds the error that can be attributed to the neglect of such core correlation effects.

Table 5 compares the attributes of the stationary points of the DMBE/CBS PES with those of other theoretical potentials for ground state NH_2, especially the recent work of Varandas et al.[16] as well as work of Ho et al.[26] The predicted geometry, energy, and vibrational frequencies of the stationary points from DMBE/CBS PES are fairly in good agreement with the results calculated from a fit to a dense grid of CBS(T,Q)/MRCI(Q) points near the stationary points. It may be due to the fact that the special weights having been attributed to the points close to stationary points in the least-squares fitting procedure.

For C_{2v} insertion of $N(^2D)$ into H_2, the DMBE/CBS PES predicts a barrier height only 0.2kcal mol^{-1} lower than the RKHS PES of Ho et al.,[26] 0.57kcal mol^{-1} lower than the one of 2.16kcal mol^{-1} obtained from DMBE/SEC PES. Perhaps not

Table 5. Stationary points at the valence region of $NH_2(12A'')$ PES.

Feature	R_1/a_0	R_2/a_0	R_3/a_0	E/E_h[a]	ΔV[b]	ω_1	ω_2	ω_3
Global minimum								
DMBE-CBS[c]	3.0277	1.9376	1.9376	−0.2923	−128.45	3375	3620	1596
DMBE/CBS[d]	3.0285	1.9374	1.9374	−0.2923	−128.45	3370	3557	1570
DMBE-SEC[e]	3.0288	1.9406	1.9406	−0.2858	−126.4	3377	3443	1523
DMBE/SEC[f]	3.0291	1.9405	1.9405	−0.2858	−126.4	3383	3457	1541
RKRS[g]	3.04	1.94	1.94		−126.4	3350	3436	1559
Exp.		1.9377[h]	1.9377[h]			3374[i]	3481[i]	1524[i]
C_{2v}barrier								
DMBE-CBS[c]	1.4185	4.0041	4.0041	−0.0851	1.58	4238	657[i]	372
DMBE/CBS[d]	1.4195	3.9824	3.9824	−0.0851	1.59	4256	616[i]	440
DMBE-SEC[e]	1.4203	3.9561	3.9561	−0.0809	2.16	4223	547[i]	385
DMBE/SEC[f]	1.4198	3.9349	3.9349	−0.0809	2.16	4209	499[i]	282
RKRS[g]	1.42	4.05	4.05		1.8	4240	499[i]	325
$C_{\infty v}$barrier								
DMBE-CBS[c]	1.5320	4.4130	2.8810	−0.0794	5.15	2954	1336[i]	1197[i]
DMBE/CBS[d]	1.5320	4.4130	2.8810	−0.0794	5.12	2483	1719[i]	901[i]
DMBE/SEC[f]	1.5121	4.4131	2.9010	−0.0763	5.1	2671	1455[i]	844[i]
RKRS[g]	1.54	4.47	2.93		4.8	2621	1032[i]	764[i]
$D_{\infty h}$barrier								
DMBE/CBS[d]	3.7523	1.8761	1.8761	−0.2393	−95.19	4075	7010	1596[i]
DMBE/SEC[f]	3.7390	1.8695	1.8695	−0.2320	−92.66	3676	6979	1544[i]

[a] Relative to the $N(^2D)-H-H$ asymptote.

[b] Relative to the $N(^2D)-H_2$ asymptote (in kcal mol^{-1}).

[c] Fitted to a dense grid of extrapolated CBS/MRCI(Q) /AV(T,Q)Z points.

[d] From global DMBE/CBS PES.

[e] Fitted to a dense grid of MRCI/AV *QZ* points, which is then scaled using the DMBE-SEC method [16].

[f] From global DMBE/SEC PES [16].

[g] From global RKHS PES [26].

[h] Refs. [57,58].

[i] Ref. [59].

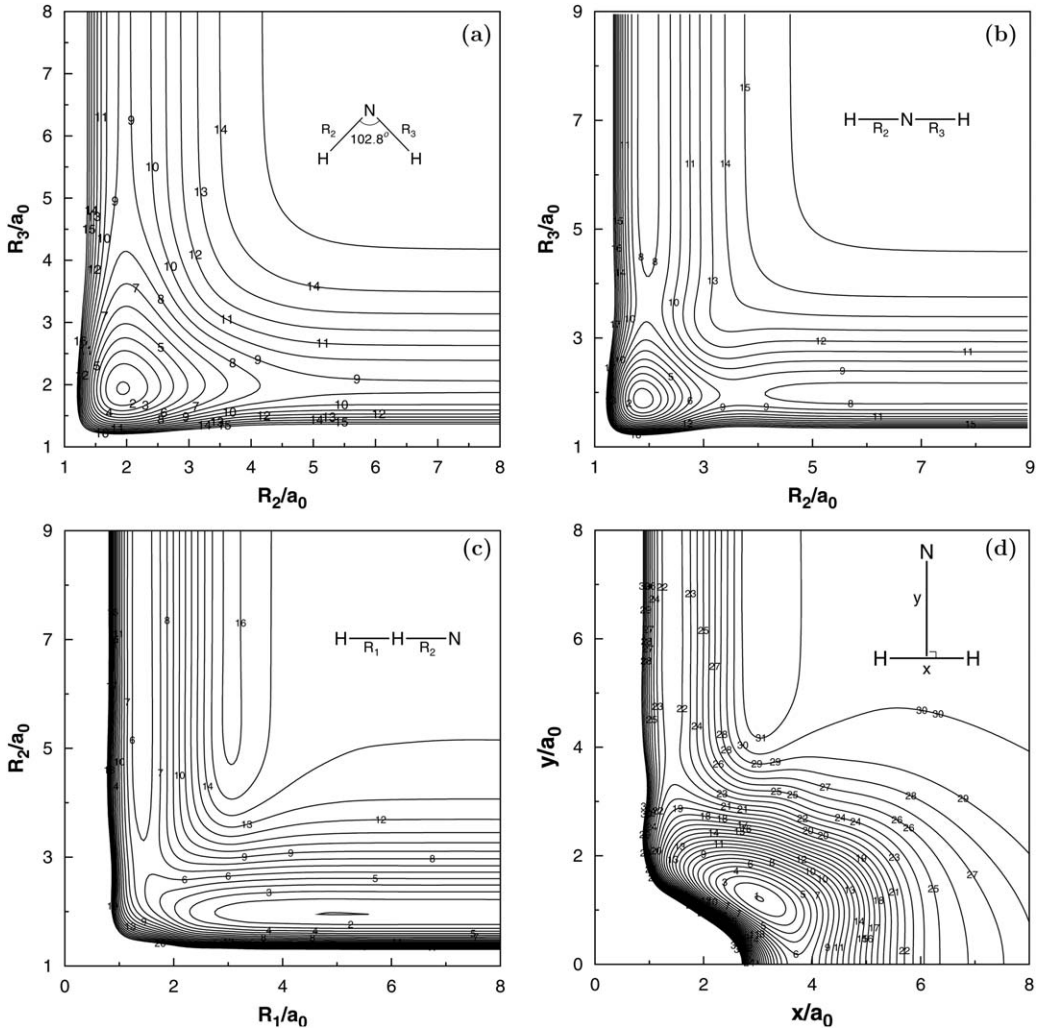

Figure 4. (a) Contour plot for bond stretching in H—N—H, keeping the included angle fixed at 102.8°. Contours are equally spaced by $0.02E_h$, starting at $-0.29E_h$. (b) Contour plot for bond stretching in linear H—N—H configurations. Contours are equally spaced by $0.015E_h$, starting at $-0.29E_h$. (c) Contour plot for bond stretching in linear H—H—N configurations. Contours are equally spaced by $0.01E_h$, starting at $-0.132E_h$. (d) Contour plot for the C_{2v} insertion of the N atom into H_2. Contours are equally spaced by $0.01E_h$, starting at $-0.292E_h$.

surprisingly, it is noted that RKHS PES from MRCI calculations by using AV *TZ* basis set, while, the DMBE/SEC PES employs a single constant scaling factor for all points calculated with the AV *QZ* basis set at the cheaper single-state level. On the other hand, the DMBE/CBS PES uses the CBS/MRCI(Q)/AV(T, Q)Z energy points.

As we can see from Table 5, the barrier heights at $C_{\infty v}$ (N−H−H) and $D_{\infty h}$ (H−N−H) geometries are in good agreement with the previous best theoretical values. Perhaps not surprisingly, as we mentioned above, it may also be due to the fact that the special weights have been attributed to the points close to stationary points in the least-squares fitting procedure, thus warranting an accurate description of the topographical features of the PES at such regions.

Figures 4 and 5 illustrate the topographical features of the $NH_2(12A')$ DMBE/SEC PES. Clearly, it has a smooth and correct behavior over the whole configuration space. Also visible from these plots are its major stationary points: C_{2v}, $C_{\infty v}$, and $D_{\infty h}$ barriers, and the global minimum. Specifically, panel (a) of Figure 4 shows the contour plot for bond stretching in H—N—H keeping the included angle fixed at 102.8°. The prominent feature from panel (a) of Figure 4 is the global minimum, which corresponds to the point of minimum energy at 102.8° in the optimized bending plot of Figure 3a. Figure 4b shows a contour plot for linear H—N—H stretch. The notable feature from this plot is the existence of a $D_{\infty h}$ linear saddle point located at $R_{NH} = 1.8761a_0$ with an energy of 33.26kcal mol^{-1} above the global minimum of $NH_2(12A')$ but still 95.19kcal mol^{-1} below the energy of the $N(^2D)-H_2$ asymptote. This compares well with the DMBE/SEC PES, where the saddle point is predicted to occur at $R_{NH} = 1.8695a_0$ with an energy of 33.74 kcal mol^{-1} above the global minimum and 92.66 kcal mol^{-1} below the reactants asymptote. The major features of the DMBE/CBS PES for collinear N—H—H are illustrated in Figure 4c. As seen, the $C_{\infty v}$ saddle point is found to have a geometry with $R_{HH} = 1.5320a_0$ and $R_{NH} = 4.4130a_0$ and a barrier height of 5.12kcal mol^{-1}. This compares with the homologous values of $R_{HH} = 1.5121a_0$, $R_{NH} = 4.4131a_0$, and 5.1kcal mol^{-1} for the

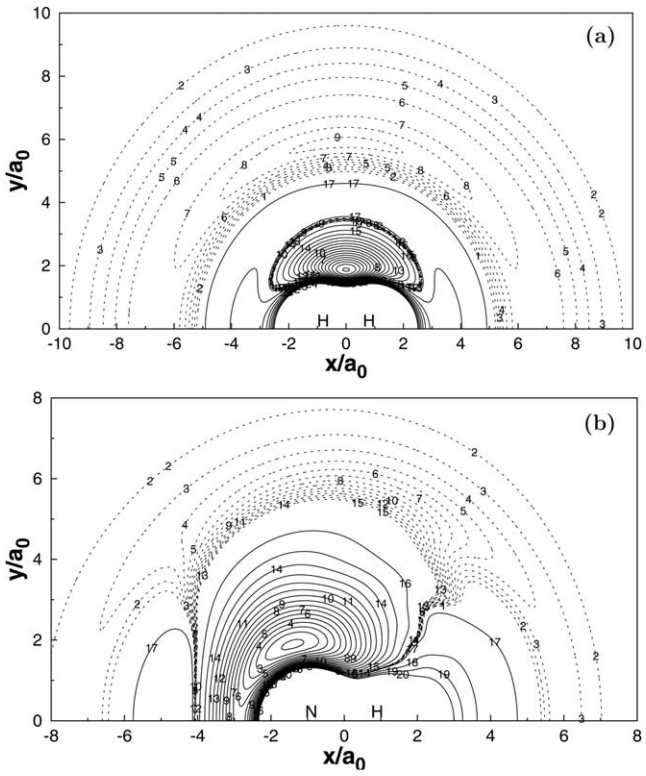

Figure 5. (a) Contour plot for an N atom moving around a H_2 molecule fixed at the equilibrium geometry $R_1 = 1.401a_0$ and lying along the *X*-axis with the center of the bond fixed at the origin. Contours are equally spaced by $0.005E_h$, starting at $-0.167E_h$. Shown in dashes are contours equally spaced by $-0.0001E_h$, starting at $-0.0876045E_h$. (b) Contour plot for a H atom moving around an NH molecule fixed at the equilibrium geometry $R_{NH} = 1.960a_0$ and lying along the *X*-axis with the center of the bond fixed at the origin. Contours are equally spaced by $0.01E_h$, starting at $-0.29E_h$. Shown in dashes are contours equally spaced by $-0.00015E_h$, starting at $-0.131702E_h$.

DMBE/SEC PES. In turn, Figure 4d shows a contour plot for the C_{2v} insertion of the nitrogen atom into the hydrogen molecule. Visible from this plot are the stationary points corresponding to C_{2v} and $D_{\infty h}$ barriers, and the global minimum. Figure 5a shows a contour plot for an N atom moving around a H_2 molecule fixed at the equilibrium geometry $R_1 = 1.401a_0$ and lying along the *X*-axis with the center of the bond fixed at the origin. The corresponding plot for H atom moving around a NH molecule with its bond distance fixed at $R_{NH} = 1.960a_0$ is shown in Figure 5b. The two plots clearly show a smooth behavior both at short- and long-range regions, which was fitted such as to provide a reliable description of the van der Waals minimum for $N(^2D)-H_2$ and NH $(X^3\Sigma^-)-H$ interaction. Table 6 reports the attributes (equilibrium geometry, vibrational frequencies, and energy relative to the atom–diatom asymptote) of the van der Waals stationary points of the DMBE/CBS PES. The properties of van der Waals well should be important for discussing the accuracy of the surface at low collision energies. In fact, the most stable structure of the reactant van der Waals complex is different from previous results. The spin-orbit effects are generally estimated using relatively small basis sets and CI under the assumption that spin-orbit effects will be insensitive to the size of basis

Table 6. Attributes of $N(^2D)-H_2$ and NH $(X^3\Sigma^-)-H$ van der Waals stationary points.

Feature	C_{2v} N···H_2 min[a]	Linear N···H—H TS[b]	Linear H···H—N TS[c]
R_1/a_0	1.4072	1.4069	4.9155
R_2/a_0	5.9505	6.9404	6.8817
R_3/a_0	5.9505	5.5335	1.9662
ΔV	−0.5222[c]	−0.3643[c]	−0.2592[d]
ω_1(intra)/cm^{-1}	4350	4401	3255
ω_2(inter)/cm^{-1}	170	125	207
ω_3(bend)/cm^{-1}	102	116 *i*	38 *i*

[a] Van der Waals minimum.
[b] Van der Waals transition state.
[c] Relative to the $N(^2D)-H_2$ asymptote (in kcal mol^{-1}).
[d] Relative to the NH $(X^3\Sigma^-)-H$ asymptote (in kcal mol^{-1}).

set and the method. It suffices to indicate at this point that the uniform USTE scheme[32,36] has been utilized on this endeavor for the dynamical correlation energy, by far the most difficult contribution to obtain accurately via *ab initio* techniques. As usual in DMBE theory, the DMBE/CBS PESs show the correct long-range behavior at all dissociation limits.[31,34]

All major topographical features of the PES are probably better viewed in the relaxed triangular plot[60] of Figure 6 utilizing scaled hyperspherical coordinates ($\beta^* = \beta/Q$ and $\gamma^* = \gamma/Q$):

$$\begin{pmatrix} Q \\ \beta \\ \gamma \end{pmatrix} = \begin{pmatrix} 1 & 1 & 1 \\ 0 & \sqrt{3} & -\sqrt{3} \\ 2 & -1 & -1 \end{pmatrix} \begin{pmatrix} {R_1}^2 \\ {R_2}^2 \\ {R_3}^2 \end{pmatrix} \quad (15)$$

Clearly visible are the equivalent stationary structures corresponding to the $C_{\infty v}$, C_{2v}, and $D_{\infty h}$ barriers, and the global minimum (labeled GM in Fig. 6).

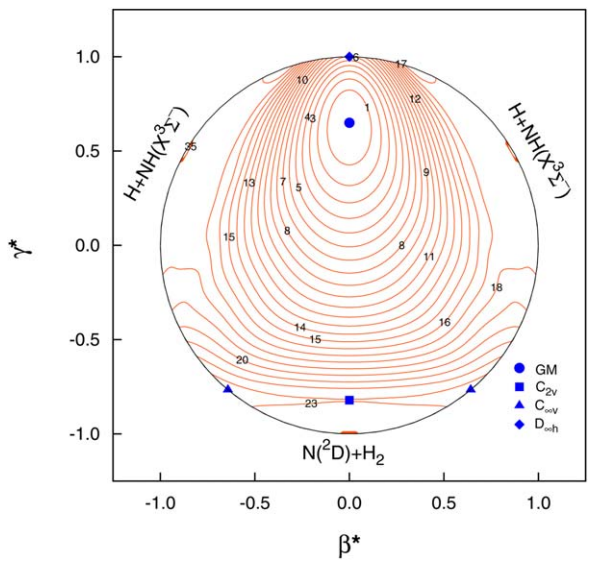

Figure 6. Relaxed triangular plot of DMBE PES of the present work in hyperspherical coordinates. Contours are equally spaced by $0.09E_h$, starting at $-0.2923E_h$. Also indicated are the various stationary points.

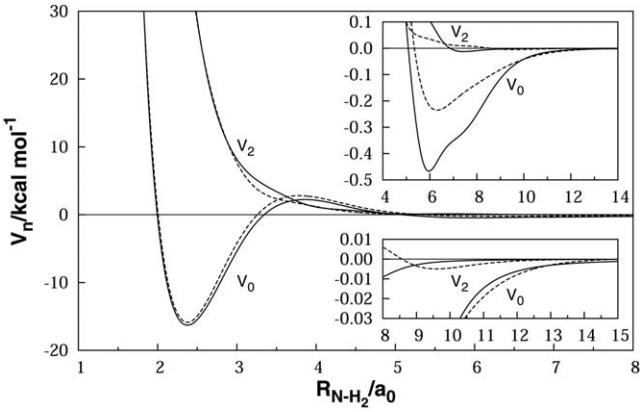

Figure 7. Isotropic (V_0) and leading anisotropic (V_2) components of the N—H_2 interaction potential, with the diatomic molecule fixed at the equilibrium geometry. continuous line, DMBE/CBS; dashed line, DMBE/SEC obtained by Varandas et al. [16]. The axes in all panels have the same units.

In turn, Figure 7 shows the isotropic and leading anisotropic components of the N—H_2 interaction potential, two important quantities of relevance in atom–diatom scattering.[61] Specifically, the isotropic potential V_0 determines how close on average the atom and molecule can approach each other, while the magnitude of V_2 indicates whether or not the molecule prefers to orient its axis along the direction of the incoming atom: a negative value favors the collinear approach while a positive value favors the approach through an isosceles triangular geometry. The barrier in V_0 located near $3.86a_0$ (see Fig. 7) corresponds to the C_{2v} transition state, as corroborated by the positive value of V_2 at such a distance. This compares well with the one of $3.78a_0$ from the DMBE/SEC PES. Correspondingly, the negative sign of V_2 at distances larger than $6.86a_0$ indicates that the van der Waals interaction energy is larger for such collinear geometries (see above insert of Fig. 7) as one would expect from the larger polarizability of the hydrogen molecule along the internuclear axis. Note, however, that the anisotropy is positive at the region of the van der Waals minimum in the isotropic potential, this is due to the van der Waals minimum associated to the T-shaped van der Waals structure. This basically coincides with DMBE/SEC, but contrasts with the RKHS surface, which predicts the van der Waals minimum at a collinear geometry. Note that the N+H_2 reaction has been shown to display a preference for the insertion mechanism, and hence such subtle details may have practical implications for scattering calculations, especially at low collision energies.

Finally, it must be stressed that to study RT coupling effects between both DMBE/CBS PESs, the excited-state $1^2A'$ DMBE/CBS potential can easily be made to degenerate with the present ground state $1^2A''$ DMBE/CBS potentials by using the switching function formalism reported in Ref. [31].

Quantum Wave Packet Dynamics Study Performed for the $N(^2D)+H_2(X^1\Sigma_g^+)$ Reaction

On the new PES, a quantum wave packet calculation was performed for the reaction. In our calculations, the Coriolis coupling effect is taken into account. The total integral cross section (ICS) and total differential cross section (DCS) were calculated using TDWP method based on the second-order split operator algorithm. The details of the method have been presented in others studies.[62,63] The reactant Jacobi coordinates (R, r, γ) were employed. The corresponding Hamiltonian for a give total angular momentum J can be written as

$$\hat{H} = -\frac{\hbar^2}{2\mu_R}\frac{\partial^2}{\partial R^2} - \frac{\hbar^2}{2\mu_r}\frac{\partial^2}{\partial r^2} + \frac{(J-j)^2}{2\mu_R R^2} + \frac{j^2}{2\mu_r r^2} + V \tag{16}$$

where μ_R and μ_r are the corresponding reduced masses for the radial Jacobi coordinates, respectively. J is the total angular momentum operator, and j is the rotational angular momentum operator of BC diatomic molecule in reaction of A + BC→AB + C.

By substituting the scattering matrix in the helicity representation into the standard formulas, we obtain the total ICS[64]

$$\sigma_{v_v j_v \leftarrow v_0 j_0} = \frac{\pi}{(2j_0+1)K^2_{v_0 j_0}} \sum_{K_v} \sum_{K_0} \sum_{J} (2J+1) \left| S^J_{v_v j_v K_v \leftarrow v_0 j_0 K_0} \right|^2 \tag{17}$$

and the total differential cross section[64]

$$\frac{d\sigma_{v_v j_v \leftarrow v_0 j_0}(\theta, E)}{d\Omega} = \frac{1}{2j_0+1} \sum_{K_v} \sum_{K_0} \left| \frac{1}{2iK^2_{v_0 j_0}} \sum_{J} (2J+1) d^J_{K_v K_0}(\theta) S^J_{v_v j_v K_v \leftarrow v_0 j_0 K_0} \right|^2 \tag{18}$$

where θ is the scattering angle between the incoming reactants and the scattered products.

On the new PES, a quantum wave packet calculation was performed for $N(^2D)+H_2(X^1\Sigma_g^+)(v=0, j=0) \rightarrow NH(X^3\Sigma^-)+H(^2S)$ reaction. In Figure 9, initial state-specified $(v=0, j=0)$ total reaction probabilities at different total angular momentum quantum number J values are displayed as a function of the collision energy. For each J value, threshold exists, which is attributed to the tiny barrier (68.5 meV) along the minimum energy reactive path. Threshold gets larger with the increase of the J value due to the emergence of centrifugal barrier. With collision energy increasing, the value of reaction probability increases rapidly to a plateau, and then oscillates around a stable value. For $J = 0$, there are two sharp peaks at the collision energy near the height of barrier, and similar peaks are observed by others near this region.[65–67] When the collision energy equals to the height of the barrier, the classical motion along the reaction coordinate will stop leading collision time delay. In quantum mechanics, bottleneck states would exist near the top of the potential barrier which could lead to the oscillation of reaction probability. The existence of the peaks probably is the signature of barrier resonance. $J = 50$ is taken as the maximum total angular momentum quantum number to calculate ICSs, and threshold energy for $J = 50$ is about 0.75 eV. In calculation of cross sections, energy of 0.75 eV is the upper limit of collision energy. Figure 10 shows the ICS from our calculations using the S-matrix method as well as results

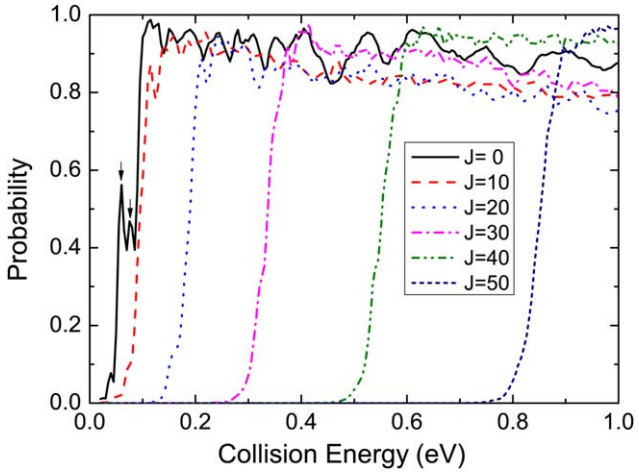

Figure 8. Total reaction probability as a function of the collision energy for the reaction of $N(^2D)+H_2\left(X^1\Sigma_g^+\right)(v=0,j=0) \rightarrow NH\,(X^3\Sigma^-)+H(^2S)$ for the total angular momentum J=0, 10, 20, 30, 40, and 50.

from previous quantum calculations employing Ho PES[65] and Varandas PES.[68] The figure shows that nearly all of these results agree with each other. Because of existence of a tiny barrier along the minimum energy path on the three PESs, threshold exists in all ICSs as showing in the figure. The threshold of our results is smaller due to the lower energy barrier (68.5 meV) on our PES comparing with Ho PES (78 meV) and Varandas PES (94 meV). With increasing energy, the values of the three ICSs get larger from zero rapidly, and the speed of increase becomes slower gradually. At higher collision energy, our ICS stays a fixed value with tiny oscillation, but the ICS obtaining from Varandas PES still maintains obvious rate of growth with larger oscillation. There are oscillations with step-like feature on the curve of these ICSs at collision energy from threshold energy to 0.3 eV, and similar oscillations are also addressed in the reaction of F+HD → HF +D by Skodje et al.[11,69] These oscillations might well be a Feshbach-type resonance signature in the ICS like F+HD → HF +D reaction, as there are enough deep potential well on these PESs to support several quantum states. Total DCS defines the angular distribution of the product and contains much detailed information of a reactive scattering event. In Figure 8, we compare the DCSs obtained from the earlier Quantum (QM) results on the Pederson PES and Ho PES at 0.165 eV[70,72] with that obtained on the new PES, and these theoretical distributions are similar. The experimental result[70] is also included in the figure in arbitrary units. Both the experimental distribution and our calculated result show that products scatter in forward and backward directions, which is a typical feature for complex-forming reactions.

Concluding Remarks

A global single-sheeted adiabatic DMBE PES has been reported for ground state of NH_2 on the basis of a least-squares fit to accurate *ab initio* MRCI(Q) energies calculated using AV *TZ* and AV *QZ* basis sets subsequently extrapolated to the CBS limit. The various topographical features of the novel PES obtained via an analytical fit with DMBE theory have been carefully compared with other realistic PESs available in the literature. They can both be recommended for dynamics studies of the $N(^2D)+H_2$ reaction and as building blocks for constructing the DMBE/CBS PESs of larger nitrogen/hydrogen-containing systems. In turn, this new surface can be using for studying the RT degeneracy to ensure an accurate match of the $1^2A''$ and $1^2A'$ DMBE/CBS PESs of NH_2 at linear $D_{\infty h}$ geometries and at asymptotic regions. We carried out theoretical study of $N(^2D)+H_2(X^1\Sigma_g^+)(v=0,j=0)$ and $NH\,(X^3\Sigma^-)+H(^2S)$ reaction using the method of quantum wave packet on the new PES. Reaction probabilities, ICSs, and DCSs have been obtained and analyzed. The existence of threshold is attributed to the barrier along the minimum energy reactive path. There are two sharp peaks at collision energy near the height of barrier on the reaction probability curve for $J = 0$. In the calculation, the

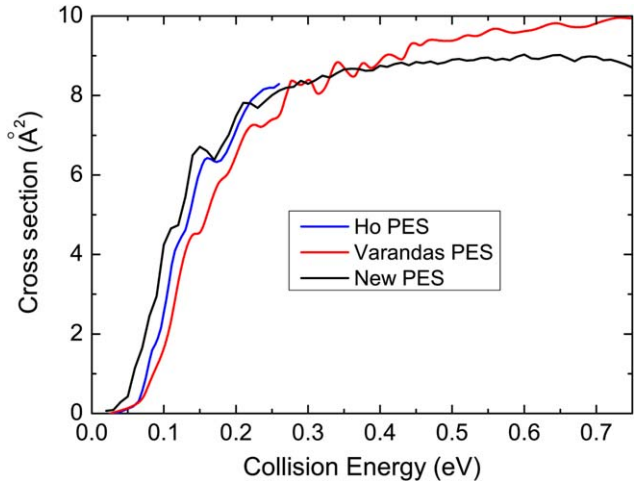

Figure 9. Integral cross sections of reaction of $N(^2D)+H_2\left(X^1\Sigma_g^+\right)(v=0,j=0) \rightarrow NH\,(X^3\Sigma^-)+H(^2S)$ as a function of collision energy, from the current calculations and previous calculations employing QM method on Ho PES [65] and Varandas PES [68]. [Color figure can be viewed in the online issue, which is available at wileyonlinelibrary.com]

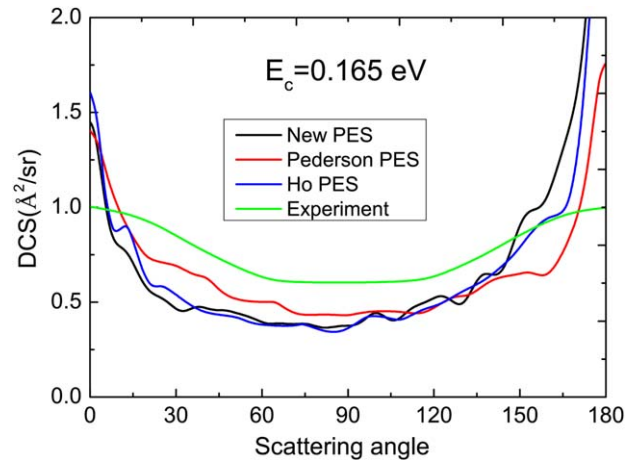

Figure 10. Differential cross sections of $N(^2D)+H_2\left(X^1\Sigma_g^+\right)(v=0,j=0) \rightarrow NH\,(X^3\Sigma^-)+H(^2S)$ reaction. Red line: QM results calculated on Pederson PES [70]. Blue line: QM results calculated on Ho PES [71]. Green line: experimental results [70] in arbitrary units. [Color figure can be viewed in the online issue, which is available at wileyonlinelibrary.com]

reaction is a typical forward and backward scatter agreeing with the experimental result.

Acknowledgment

The authors are grateful to A. J. C. Varandas for useful discussions and his Code of DMBE/SEC PES.

Keywords: potential energy surface · ab initio · double many-body expansion · CBS limit

How to cite this article: Y. Li, J. Yuan, M. Chen, F. Ma, M. Sun, *J. Comput. Chem.* **2013**, *34*, 1686–1696. DOI: 10.1002/jcc.23303

[1] R. P. Saxon, B. H. Lengsfield, III, B. Liu, *J. Chem. Phys.* **1983**, *78*, 312.
[2] J. A. Dodd, S. J. Lipson, D. J. Flanagan, W. A. M. Blumberg, J. C. Pearson, B. D. Green, *J. Chem. Phys.* **1991**, *94*, 4301.
[3] H. Umemoto, K. Matsumoto, *J. Chem. Phys.* **1996**, *104*, 9640.
[4] H. Umemoto, T. Asai, Y. Kimura, *J. Chem. Phys.* **1997**, *106*, 4985.
[5] M. Alagia, N. Balucani, L. Cartechini, P. Cachavecchia, G. G. Volpi, L. A. Pederson, G. C. Schatz, G. Lendvay, L. B. Harding, T. Hollebeek, T.-S. Ho, H. Rabitz, *J. Chem. Phys.* **1999**, *110*, 8857.
[6] A. N. Wright, C. A. Winkler, Active Nitrogen; Academic: New York, **1968**.
[7] T. Takayanagi, Y. Kurosaki, K. Yokoyama, *Chem. Phys. Lett.* **2000**, *321*, 106.
[8] R. J. Buenker, M. Perić, S. D. Peyerimhoff, R. Marian, *Mol. Phys.* **1981**, *43*, 987.
[9] P. Jensen, R. J. Buenker, G. Hirsch, S. N. Rai, *Mol. Phys.* **1990**, *70*, 443.
[10] K. Funken, B. Engels, S. D. Peyerimhoff, F. Grein, *Chem. Phys. Lett.* **1990**, *172*, 180.
[11] T. Suzuki, Y. Shihira, T. Sato, H. Umemoto, S. Tsunashima, *J. Chem. Soc. Faraday Trans.* **1993**, *89*, 995.
[12] R. Vetter, L. Zülicke, A. Koch, E. F. van Dishoeck, S. D. Peyerimhoff, *J. Chem. Phys.* **1995**, *104*, 5558.
[13] T. Takayanagui, H. Kobayashi, S. Tsunashima, *J. Chem. Soc. Faraday Trans.* **1996**, *92*, 1311.
[14] Z. Qu, H. Zhu, R. Schinke, L. Adam, W. Hack, *J. Chem. Phys.* **2005**, *122*, 204313.
[15] T. S. Chu, R. F. Lu, K. L. Han, X. N. Tang, H. F. Xu, C. Y. Ng, *J. Chem. Phys.* **2005**, *122*, 244322.
[16] A. J. C. Varandas, L. A. Poveda, *Theor. Chem. Acc.* **2006**, *116*, 404.
[17] T. S. Chu, K. L. Han, A. J. C. Varandas, *J. Phys. Chem. A.* **2006**, *110*, 1666.
[18] L. Adam, W. Hack, G. C. McBane, H. Zhu, Z.-W. Qu, *R. Schinke J. Chem. Phys.* **2007**, *126*, 034304.
[19] S. L. Zhou, D. Xie, S. Y. Lin, H. Guo, *J. Chem. Phys.* **2008**, *128*, 224316.
[20] H. S. Zhai, K. L. Han, *J. Chem. Phys.* **2011**, *135*, 104314.
[21] T. S. Chu, Y. Zhang, K. L. Han, *Int. Rev. Phys. Chem.* **2006**, *25*, 201.
[22] T. S. Chu, K. L. Han, *Phys. Chem. Chem. Phys.* **2008**, *10*, 2431.
[23] T. S. Chu, K. L. Han, *J. Phys. Chem. A.* **2005**, *109*, 2050.
[24] P. Y. Zhang, S. J. Lv, *Commun. Comput. Chem.* **2013**, *1*, 63.
[25] H. Kobayashi, T. Takayanagi, K. Yokoyama, T. Sato, S. Tsunashima, *J. Chem. Soc. Faraday Trans.* **1995**, *91*, 3771.
[26] T.-S. Ho, H. Rabitz, F. J. Aoiz, L. Bañares, S. A. Vázquez, L. B. Harding, *J. Chem. Phys.* **2003**, *119*, 3063.
[27] L. A. Pederson, G. C. Schatz, T. Ho, T. Hollebeek, H. Rabitz, L. B. Harding, *J. Chem. Phys.* **1999**, *110*, 9091.
[28] L. Pederson, G. Schatz, T. Hollebeek, T.-S. Ho, H. Rabitz, *L. B. Harding J. Phys. Chem. A* **2000**, *104*, 2301.
[29] S. L. Zhou, Z. Li, D. Xie, S. Y. Lin, H. Guo, *J. Chem. Phys.* **2009**, *130*, 184307.
[30] A. J. C. Varandas, *J. Chem. Phys.* **1989**, *90*, 4379.
[31] Y. Q. Li, A. J. C. Varandas, *J. Phys. Chem. A.* **2010**, *114*, 9644.
[32] A. J. C. Varandas, *J. Chem. Phys.* **2007**, *126*, 244105.
[33] Y. Z. Song, A. J. C. Varandas, *J. Chem. Phys.* **2009**, *130*, 134317.
[34] Y. Q. Li, A. J. C. Varandas, *Int. J. Quantum Chem.* **2012**, *112*, 2932.
[35] T. H. Dunning, Jr, *J. Chem. Phys.* **1989**, *90*, 1007.
[36] A. J. C. Varandas, *J. Chem. Phys.* **2007**, *127*, 114316.
[37] H.-J. Werner, P. J. Knowles, *J. Chem. Phys.* **1988**, *89*, 5803.
[38] P. J. Knowles, H.-J. Werner, *Chem. Phys. Lett.* **1988**, *145*, 514.
[39] H.-J. Werner, P. J. Knowles, G. Knizia, F. R. Manby, M. Schütz, P. Celani, T. Korona, R. Lindh, A. Mitrushenkov, G. Rauhut, K. R. Shamasundar, T. B. Adler, R. D. Amos, A. Bernhardsson, A. Berning, D. L. Cooper, M. J. O. Deegan, A. J. Dobbyn, F. Eckert, E. Goll, C. Hampel, A. Hesselmann, G. Hetzer, T. Hrenar, G. Jansen, Köppl, C., Y. Liu, A. W. Lloyd, R. A. Mata, A. J. May, S. J. McNicholas, W. Meyer, M. E. Mura, A. Nicklass, D. P. O'Neill, P. Palmieri, K. Pflüger, R. Pitzer, M. Reiher, T. Shiozaki, H. Stoll, A. J. Stone, R. Tarroni, T. Thorsteinsson, M. Wang, A. Wolf, Molpro, version 2010.1, a package of ab initio programs, **2010**.
[40] A. Karton, J. M. L. Martin, *Theor. Chim. Acta* **2006**, *115*, 330.
[41] A. J. C. Varandas, *J. Chem. Phys.* **2000**, *113*, 8880.
[42] A. J. C. Varandas, *Chem. Phys. Lett.* **2007**, *443*, 398.
[43] A. J. C. Varandas, *J. Chem. Phys.* **2008**, *129*, 234103.
[44] A. J. C. Varandas, *Chem. Phys. Lett.* **2008**, *463*, 225.
[45] A. J. C. Varandas, *J. Comput. Chem.* **2009**, *30*, 379.
[46] Y. Q. Li, A. J. C. Varandas, *J. Phys. Chem. A.* **2010**, *114*, 6669.
[47] Y. Q. Li, Y. Z. Song, P. Song, Y. Z. Li, Y. Ding, M. T. Sun, F. C. Ma, *J. Chem. Phys.* **2012**, *136*, 194705.
[48] L. A. Poveda, A. J. C. Varandas, *Phys. Chem. Chem. Phys.* **2005**, *7*, 2867.
[49] A. J. C. Varandas, J. Silva, *J. Chem. Soc. Faraday Trans.* **1992**, *88*, 941.
[50] A. J. C. Varandas, *J. Chem. Phys.* **1996**, *105*, 3524.
[51] A. J. C. Varandas, S. P. J. Rodrigues, *J. Phys. Chem A.* **2006**, *110*, 485.
[52] E. Martínez-Núñez, A. J. C. Varandas, *J. Phys. Chem. A.* **2001**, *105*, 5923.
[53] A. J. C. Varandas, J. N. Murrell, *Faraday Discuss. Chem. Soc.* **1977**, *62*, 92.
[54] A. J. C. Varandas, J. N. Murrell, *Chem. Phys. Lett.* **1981**, *88*, 440.
[55] M. R. Pastrana, L. A. M. Quintales, J. Brandão, *A. J. C. Varandas J. Phys. Chem.* **1990**, *94*, 8073.
[56] G. Duxbury, *A. Alijah J. Mol. Spectrosc.* **2002**, *211*, 31.
[57] J. Demaison, L. Margulés, J. Boggs, *Phys. Chem. Chem. Phys.* **2003**, *5*, 3359.
[58] K. Dressler, D. A. Ramsay, *Phil. Trans. Roy. Soc.* **1959**, *251A*, 553.
[59] W. Gabriel, G. Chambaud, P. Rosmus, S. Carter, N. Handy, *Mol. Phys.* **1994**, *6*, 1445–1461.
[60] A. J. C. Varandas, *Chem. Phys. Lett.* **1987**, *138*, 455.
[61] A. J. C. Varandas, *J. Chem. Phys.* **1979**, *70*, 3786.
[62] Z. G. Sun, H. Guo, D. H. Zhang, *J. Chem. Phys.* **2010**, *132*, 084112.
[63] Z. G. Sun, S. Y. Lee, H. Guo, D. H. Zhang, *J. Chem. Phys.* **2009**, *130*, 174102.
[64] J. Z. H. Zhang, W. H. Miller, *J. Chem. Phys.* **1989**, *91*, 1528.
[65] S. Y. Lin, H. Guo, *J. Chem. Phys.* **2006**, *124*, 031101.
[66] B. J. Rao, S. Mahapatra, *J. Chem. Phys.* **2007**, *127*, 244307.
[67] J. F. Castillo, N. Bulut, L. Banares, F. Gogtas, *Chem. Phys.* **2007**, *332*, 119.
[68] A. J. C. Varandas, T. S. Chu, K. L. Han, P. J. S. B. Caridade, *Chem. Phys. Lett.* **2006**, *421*, 415.
[69] R. T. Skodje, D. Skouteris, D. E. Manolopoulos, S. H. Lee, F. Dong, K. Liu, *J. Chem. Phys.* **2000**, *112*, 4536.
[70] N. Balucani, P. Casavecchia, L. Banares, F. J. Aoiz, T. Gonzalez-Lezana, P. Honvault, J. M. Launay, *J. Phys. Chem. A.* **2006**, *110*, 817.
[71] S. Y. Lin, L. Banares, H. Guo, *J. Phys. Chem. A.* **2007**, *111*, 2316.
[72] S. Y. Lin, L. Banares, H. Guo, *J. Chem. Phys.* **2007**, *111*, 2376.

Received: 20 December 2012
Accepted: 8 April 2013
Published online on 10 May 2013